

Dual Quasi-Bound States in the Continuum Modes for Optical Activity Manipulation

Dongfang Shen , Xingang Ren , Member, IEEE, Qing Ci, Kaikun Niu, Siliang Wang, and Zhixiang Huang , Senior Member, IEEE

Abstract—Quasi-bound states in the continuum (quasi-BIC) are a particular resonant state, which can be regulated by the degree of symmetry breaking in nanostructures. Here, we propose a four-fold rotationally symmetric (C_{4v}) metasurface supporting the dual quasi-BIC modes. The Fano characteristics have been observed in the near-infrared region. The resonant peaks of the dual quasi-BIC modes can be adjusted flexibly and independently with a simple breaking of the structural symmetry. More importantly, the dual quasi-BIC modes demonstrate the extraordinary capability in controlling the optical activity. This work will offer us more freedom for controlling the resonance and optical activity by the quasi-BIC modes, which is promising to engineer the optical device in displaying and optics communications.

Index Terms—Quasi-bound states in the continuum, metasurface, Fano resonance, optical activity.

I. INTRODUCTION

THE BOUND states in the continuum (BIC) mode reside inside the continuous spectrum of the extended radiating state, which is a perfectly confined mode in space with a theoretically infinite lifetime [1]–[3]. Since the first report of BIC mode in photonics [4], [5], it has received intensive research interest due to the infinite quality factor (Q-factor) of BIC mode, which is a promising approach to manipulate the light-matter interactions. The strong BIC mode excited in photonic crystal slab (PhCs) is typically protected by the symmetric characteristics

at the Γ point [6], [7]. However, in practice, the BIC mode will usually turn into the quasi-BIC mode due to intrinsic material loss or broken symmetry because of the imperfect fabrication. The theoretically infinite Q-factor will become a finite value but still extremely large that is of great use in forming the super-cavity [8].

The super-cavity formed by the quasi-BIC mode is capable of manipulating the propagation and localization of electromagnetic waves. The super-cavities, e.g., sub-wavelength topological photonic [9] and insulator [10], [11], have boosted laser, grating coupler, optical antenna performance with quasi-BIC resonances. In addition, the spectral response of quasi-BIC mode reveals the sharp Fano features, which indicates the phase transition can be engineered through modifying the structural parameters or the excitation conditions [7], [12]–[15]. The abrupt phase transition resembling the functionality arisen by the chiral molecules or chiral structures is of great use to achieve the strong optical activity [16], [17].

As we know, the linear polarized light can be expressed as the superposition of the left-circularly polarized (LCP) and right-circularly polarized (RCP) light. When the light with linear polarization passes through the optical chiral material or the structure with spiral features, the LCP and RCP light will produce different phase delays, and the generation of the phase difference between the LCP and RCP light plays an essential role in the polarization control, nonlinear optics [18] and molecular biology [19]. However, the chiro-optical interactions are feeble in structure without chiral materials. It is desirable to deliver a simple and tunable chiral structure toward very large Q-factor and multiple tunable resonances. The strong chiro-optical interactions have potential advantages to modulate the optical activity, particularly for biological and chemical sensing [20], [21], imaging, and holography [22], [23].

In this work, we have proposed a fourfold rotationally symmetric (C_{4v}) metasurface composed of a cross-shaped silicon resonator. The C_{4v} metasurface with a square lattice supports the dual quasi-BIC modes in the near-infrared region. With the introduction of symmetry breaking in the plane of incidence, the incident light almost transmits through the metasurface at dual quasi-BIC mode frequencies because of the abrupt phase retardation by the quasi-BIC modes [24]. By adjusting the degree of the geometrical asymmetry, the BIC mode enables the control of optical activity with the rotation angle covering from 0 to 180° [25], [26]. The variations of the optical activity are well explained by the Jones matrix referring to its polarization state.

Manuscript received September 13, 2021; revised October 18, 2021; accepted October 23, 2021. Date of publication October 27, 2021; date of current version November 9, 2021. This work was supported in part by the National Natural Science Foundation of China under Grants 62171001, 61701003, 6210011825, 61901001, 61701001, U20A20164, 61871001, 61971001 and 6140209, in part by the Anhui Province under Grants 2108085MF198, 1808085QF179, 21080850QF261, 1908085QF259, 1908085QF251, in part by the University Synergy Innovation Program of Anhui Province under Grants GXXT-2020-050, GXXT-2020-051, and in part by the Open fund for Discipline Construction, Institute of Physical Science and Information Technology, Anhui University, and Postdoctoral Science Foundation founded project of Anhui Province under Grant 2019B348. (Dongfang Shen and Xingang Ren equally contributed to this work.) (Corresponding author: Xingang Ren.)

Dongfang Shen, Xingang Ren, Qing Ci, Kaikun Niu, Siliang Wang, and Zhixiang Huang are with the Information Materials and Intelligent Sensing Laboratory of Anhui Province, Institute of Physical Science and Information Technology, Anhui University, Hefei 230601, China, with Anhui Province Key Laboratory of Target Recognition and Feature Extraction, Lu'an 230601, China, and also with the Key Laboratory of Electromagnetic Environmental Sensing, Department of Education of Anhui Province, Hefei 230039, China (e-mail: 2831546153@qq.com; xgren@ahu.edu.cn; p19301123@stu.ahu.edu.cn; kkniu@ahu.edu.cn; sliang_wang@163.com; zxhuang@ahu.edu.cn).

This article has supplementary downloadable material available at <https://doi.org/10.1109/JPHOT.2021.3123094>, provided by the authors.

Digital Object Identifier 10.1109/JPHOT.2021.3123094

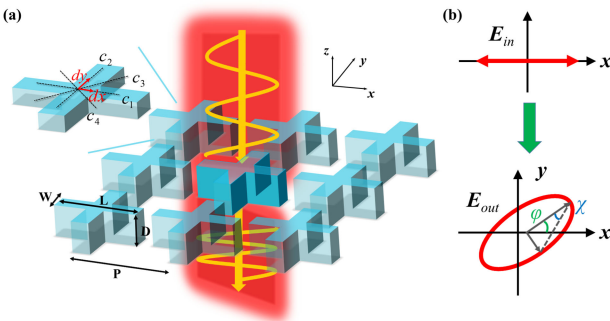


Fig. 1. (a) The schematic illustration of the C_{4v} metasurface, the geometrical parameters are listed: the periodicity is $P = 475$ nm, the length and width of lattice are $L = 370$ nm and $W = 100$ nm, and its thickness is $D = 320$ nm. The upper left Figure represents the symmetrical characteristics of the C_{4v} metasurface, and the symmetry breaking is introduced along the in-plane c_1 (x -) axis and out-of-plane c_2 (y -) axis. (b) The optical activity induced by the C_{4v} metasurface is schematically illustrated. The electric field direction is governed by the rotation angle φ and ellipticity angle χ .

The manipulations of optical activity by dual quasi-BIC modes are promising to nonlinear optical imaging, quantum information, and biological sensing.

II. DEVICE STRUCTURE AND SIMULATION

The C_{4v} metasurface is formed by a cross-shaped slab (Fig. 1), which material is silicon with the refractive index of $n_{Si} = 3.58$ in the near-infrared region. The geometrical parameters of metasurface are listed as: the periodicity of the square lattice is $P = 475$ nm, the length and width are $L = 370$ nm and $W = 100$ nm, respectively, the thickness is $D = 320$ nm. The band structure and Q-factor are calculated in the framework of finite element method by the eigenmode solver. To unveil the interactions between the C_{4v} metasurface and input light, the in-plane wave with transverse magnetic (TM) field has been adopted as the excitation source. The periodic boundary conditions are imposed in the horizontal (xoy) plane, and the perfectly matched layers (PMLs) are constructed in the vertical (z -) direction.

III. RESULTS AND DISCUSSION

The band diagram of the proposed C_{4v} metasurface has obtained across the wavelength from 910 nm to 935 nm (Fig. 2(a)) corresponding to the normalized wave vector of $k = -0.08\text{--}0.08$. The C_{4v} metasurface supports two BIC modes, i.e., at Γ point of TM1 and TM2 bands, which are located above the light cone but have different topological properties. Correspondingly, the TM2 mode has a higher Q-factor than the TM1 mode for the wavenumber $k \neq 0$. Meanwhile, the near electric-field enhancement also indicates the different properties of the topological states for the two BIC modes according to topology theory [27]. The fitted data of the Q-factor reveals the quadratic ($1/k^2$) decay concerning the distance k in the momentum space of TM1 and TM2 bands.

Without the intrinsic loss of materials or broken symmetry, the symmetry-protected BIC modes of TM1 and TM2 bands cannot be coupled into the external radiation [28]. After shifting

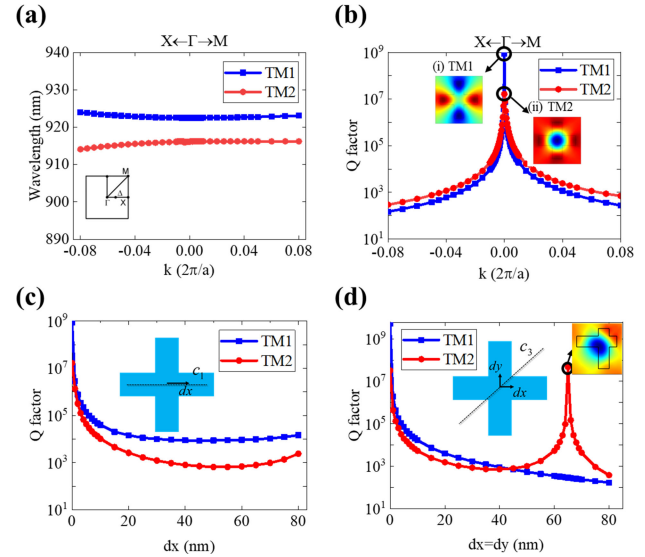


Fig. 2. (a) The band diagram of C_{4v} metasurface. (b) The variation of Q-factor with the normalized wave vector k . The inset Figs. show the electric-field enhancement at the Γ point of TM1 and TM2 bands. The Q-factor varied with the degree of broken symmetry along (c) c_1 axis with displacement in the x -direction. (d) c_3 axis with equal displacement in both x and y directions. The inset figures show the electric-field enhancement at the Γ point of TM2 bands.

of the silicon slab along the c_1 and c_3 axis with the displacement of dx and dy , respectively, the two BIC modes of the C_{4v} metasurface have transformed into the quasi-BIC modes forming the super-cavity modes. The Q-factor is substantially decayed with an increase in the degree of symmetry breaking for both TM1 and TM2 bands (Fig. 2(c), (d)). The quasi-BIC mode of TM1 and TM2 bands with different topological states in momentum space results in a different decay rate of Q-factor. Regarding the TM2 band, the Q-factor has decreased since the initial introduction of asymmetry along c_3 axis. With the further increased degree of asymmetry, an emerging peak of Q-factor has observed in the TM2 band with the displacement of $dx = dy = 65$ nm. However, the emerging peak will be disappeared after introducing the symmetry breaking along the z -axis (e.g., with different substrates below C_{4v} metasurface).

Meanwhile, we have also examined the optical transmission (Fig. 3(a)) for the C_{4v} metasurface with the broken symmetry along the in-plane c_1 axis under different displacement dx . There are two resonant peaks with 100% transmission efficiency that corresponds to the dual quasi-BIC modes of TM1 and TM2 bands. It can be observed that the resonant wavelength of the quasi-BIC mode on TM1 band shows a significant blue shift, while the quasi-BIC mode on TM2 band reveals a slight redshift. The increment of the displacement dx will induce a large spectral distance between quasi-BIC modes on TM1 and TM2 band, which will weaken the mode coupling between two quasi-BIC modes [12].

The increment of the displacement dx along in-plane c_1 axis for the C_{4v} metasurface shows the declined Q-factor, and the resonance curve reveals the Fano line shape. The phase of the transmission spectra has been extracted and shown in Fig. 3(b). Without the asymmetry, the excitation of BIC mode

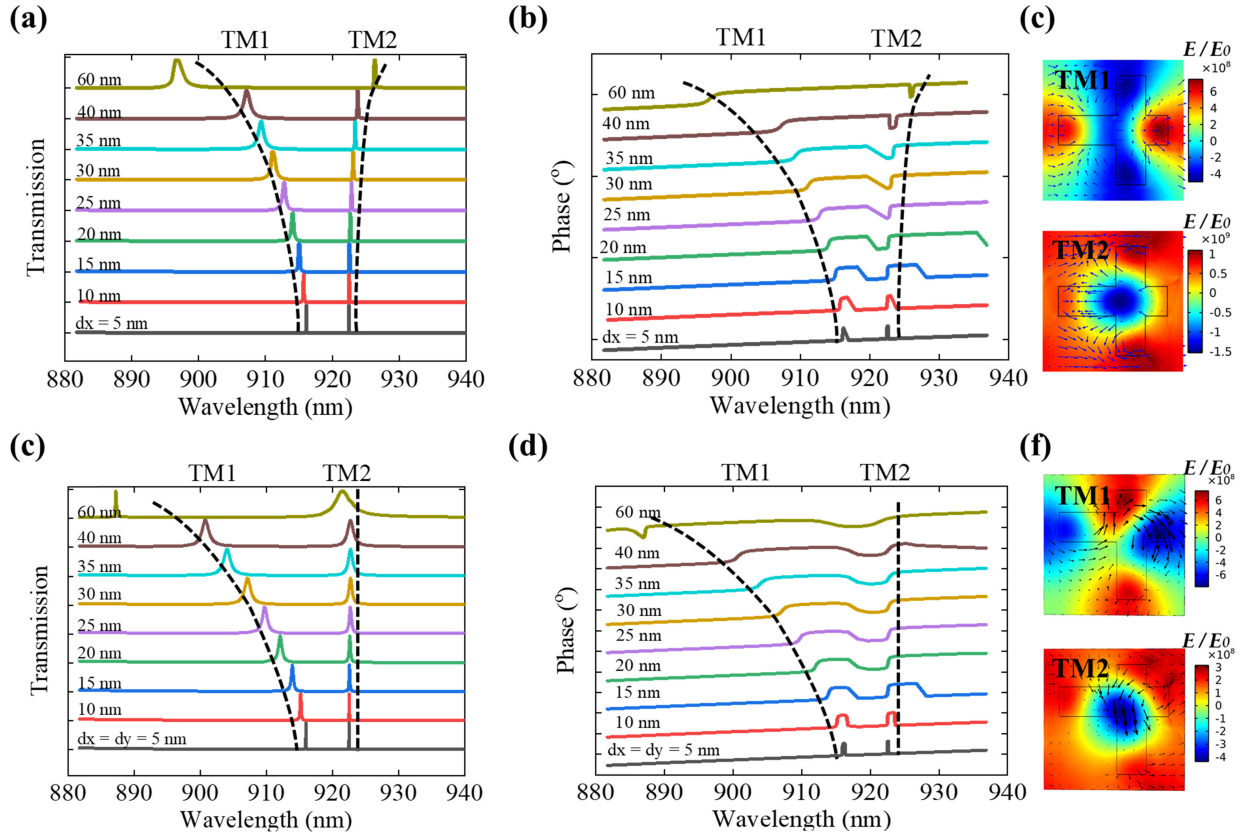


Fig. 3. (a) Transmission amplitude and (b) phase of C_{4v} metasurface with broken symmetry along c_1 axis of displacement dx , (c) The inset figures show the electric-field enhancement at the Γ point of TM1 and TM2 bands and Poynting vector of TM1 and TM2 bands at $dx = 60$ nm. (d) Transmission amplitude and (e) phase of C_{4v} metasurface with broken symmetry along c_3 axis of equal displacement $dx = dy$, (f) the electric-field enhancement and Poynting vector of TM1 and TM2 bands at $dx = dy = 60$ nm.

with theoretically infinite Q-factor is difficult, while the BIC mode will become the expected quasi-BIC mode after the introduction symmetry breaking, and the conspicuous Fano interference characteristics will be disclosed [6]. The phase retardation generated by two quasi-BIC modes reveals the tunable characteristic modulating the degree of in-plane asymmetry (Fig. 3(b)). This behavior enables the regulation of the Fano resonant line shape even the polarization states with quasi-BIC mode by engineering the asymmetry [29], which offers a novel approach for the polarization control and is promising to the optical circuit switching device, particularly for the multi-mode channel [30]. The electric field distributions of quasi-BIC mode on TM1 and TM2 bands have shown in Fig. 3(c); the arrows represent the energy flux direction of the Poynting vector that shows a dominant horizontal flow along the x -direction. The field enhancement of quasi-BIC modes well preserves resonant features of BIC modes. The existence of the symmetry breaking alters light with the confined mode into the radiative mode, which enables us to observe the resonant peaks in transmission spectrum.

When the symmetry breaking exists along both c_3 axis with the equal displacement of dx and dy , the transmission spectra of the C_{4v} metasurface are shown in Fig. 3(d). The resonant peaks of TM2 band are almost fixed at 923 nm, while the quasi-BIC mode of TM1 band reveals remarkably blue-shifted

characteristics. Introducing out-of-plane broken symmetry in C_{4v} metasurface enables the single-mode regulation and the control of the spectral distance between the two quasi-BIC resonance. The transmission phase (Fig. 3(e)) also implies different phase retardation for the two quasi-BIC modes of TM1 and TM2 bands, which are promising for multi-mode manipulation of optical circuits and fibers [31]. Fig. 3(f) shows the profiles of the electric-field enhancement at the Γ point of TM1 and TM2 bands, respectively. The two quasi-BIC modes have revealed similar patterns as compared to Fig. 3(e). However, the energy flux of the Poynting vector reveals the vortex characteristics that are different from the one with in-plane asymmetry along c_1 axis.

Regarding the polarization state, the rotation angle and the ellipticity angle are two critical parameters to characterize the transmitted light's optical activity. Therefore, we have extracted the optical rotation angle φ and ellipticity angle χ (as defined in Fig. 1) for the C_{4v} metasurface. The broken symmetry exists along the c_3 axis under different displacements dx and dy (Figs. 4 and 5). When the displacement dx changes from 10 nm to 60 nm with fixed $dy = 60$ nm, the optical rotation angle (transmission) at the quasi-BIC mode of TM1 band has a tendency to increase first and then decrease within the range of 25° to 55° (0.2 to 0.7), which indicates the direction of the electric field polarization has fallen into $\varphi = 0 \sim 90^\circ$ (i.e., quadrant I and III). Differently, the quasi-BIC mode of TM2 band has a different behavior of the

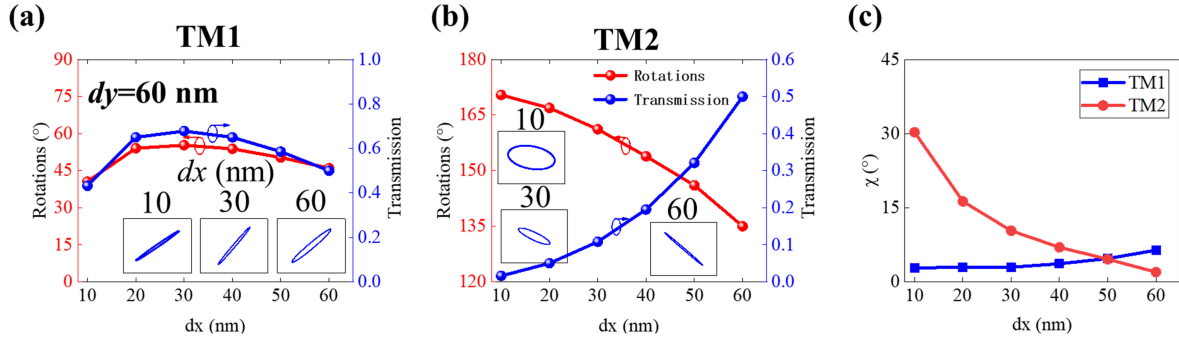


Fig. 4. The transmission amplitude (red dot line)/optical rotation angle φ (blue dot line) at the quasi-BIC modes of (a) TM1 band, (b) TM2 band, and (c) the corresponding ellipticity angle χ with fixed displacement $dy = 60$ nm, the varied asymmetrical parameter dx is along c_1 axis. The insets in (a, b) denote polarization states.

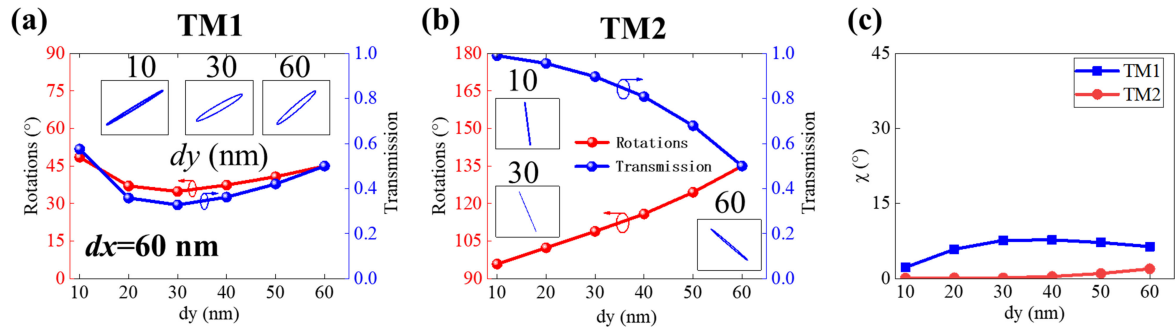


Fig. 5. The transmission amplitude/optical rotation angle φ at quasi-BIC modes of (a) TM1 band, (b) TM2 band, and (c) the corresponding ellipticity angle χ with fixed displacement $dx = 60$ nm, the varied asymmetrical parameter dy is along c_2 axis. The insets in (a, b) denote polarization states.

optical rotations due to their respective characteristics of the topological state. The optical rotation (transmission) of TM2 band is monotonically decreased from 175° to 135° (increased from 0 to 0.5), which indicates the direction of the electric field polarization falls into $\varphi = 90\text{--}180^\circ$ (i.e., quadrant II and IV).

When the displacement dy is varied from 10 nm to 60 nm (with the fixed $dx = 60$), the optical rotation and transmission show substantially different trends compared to the previous case. As shown in Fig. 5(a), the optical rotation angle of TM1 band first decreases from 65° to 30° and then climbs up to 45°. The transmission reveals a similar tendency, and the maximum amplitude of transmission is as high as 0.8 under the displacement of $dy = 10$ nm. For the TM2 band, the optical rotation angle gradually increases from 90° to 135° with the displacement dy from 10 nm to 60 nm, and the corresponding transmission decreases from 1 to 0.5. Therefore, the dual quasi-BIC modes enable us to modulate the optical activity, which offers us great freedom to manipulate the optical rotation of linearly polarized light over the entire quadrants.

Besides, the ellipticity angle of different polarization states has also examined (Fig. 4(c) and Fig. 5(c)). The results indicate that the ellipticity angle χ of TM1 band maintains a value less than 10°, which implies the linear characteristics of the transmitted light even for different optical rotation angles. Regarding the quasi-BIC mode of TM2 band, the ellipticity angle can be tuned up to $\chi = 45^\circ$ under a small displacement $dx = 10$ nm with the fixed $dy = 60$ nm, while the transmission amplitude is almost zero. With the increase of displacement

dx , the ellipticity angle will reduce to zero, implying the linear plane wave.

IV. CONCLUSION

In conclusion, we have adopted dual quasi-BIC with different topological characteristics for optical activity manipulation, and the physical properties of C_{4v} metasurface with dual quasi-BIC modes have also been explored. The quasi-BIC modes of the C_{4v} metasurface can be engineered with the degree of geometrical asymmetric perturbation, and the dual quasi-BIC modes can be independently regulated. In addition, the linearly polarized light, combined with Fano resonance, enables the outgoing beam to have controllable optical activity with the rotation angle covering from 0° to 180°. The ellipticity angle from 0° to 45°. The excited quasi-BIC mode with a high Q-factor ensures the high transmission and efficient conversion of optical activity simultaneously. The simultaneous control of dual quasi-BIC modes and optical activity promises optical communication, displaying and imaging, etc.

REFERENCES

- [1] C. W. Hsu, B. Zhen, A. D. Stone, J. D. Joannopoulos, and M. Soljačić, "Bound states in the continuum," *Nat. Rev. Mater.*, vol. 1, no. 9, pp. 1–13, 2016.
- [2] F. H. Stillinger and D. R. Herrick, "Bound states in the continuum," *Phys. Rev. A*, vol. 11, no. 2, pp. 446–454, 1975.
- [3] H. Friedrich and D. Wintgen, "Interfering resonances and bound states in the continuum," *Phys. Rev. A*, vol. 32, no. 6, pp. 3231–3242, Dec. 1985.

- [4] D. C. Marinica, A. G. Borisov, and S. V. Shabanov, "Bound states in the continuum in photonics," *Phys. Rev. Lett.*, vol. 100, no. 18, May 9, 2008, Art. no. 183902.
- [5] E. N. Bulgakov and A. F. Sadreev, "Bound states in the continuum in photonic waveguides inspired by defects," *Phys. Rev. B*, vol. 78, no. 7, 2008, Art. no. 075105.
- [6] K. Koshelev, S. Lepeshov, M. Liu, A. Bogdanov, and Y. Kivshar, "Asymmetric metasurfaces with high-Q resonances governed by bound states in the continuum," *Phys. Rev. Lett.*, vol. 121, no. 19, Nov. 9, 2018, Art. no. 193903.
- [7] C. W. Hsu *et al.*, "Observation of trapped light within the radiation continuum," *Nature*, vol. 499, no. 7457, pp. 188–191, Jul. 11, 2013.
- [8] Q. Ren *et al.*, "Multiplexing-oriented plasmon-MoS₂ hybrid metasurfaces driven by nonlinear quasi bound states in the continuum," *Opt. Exp.*, vol. 29, no. 4, pp. 5384–5396, Feb. 15, 2021.
- [9] X. Yin, J. Jin, M. Soljacic, C. Peng, and B. Zhen, "Observation of topologically enabled unidirectional guided resonances," *Nature*, vol. 580, no. 7804, pp. 467–471, Apr. 2020.
- [10] M. Autore *et al.*, "Plasmon-phonon interactions in topological insulator microrings," *Adv. Opt. Mater.*, vol. 3, no. 9, pp. 1257–1263, 2015.
- [11] L. C. Tung *et al.*, "Magneto-infrared spectroscopic study of thin Bi₂Te₃ single crystals," *Phys. Rev. B*, vol. 93, no. 8, 2016, Art. no. 085140.
- [12] M. F. Limonov, M. V. Rybin, A. N. Poddubny, and Y. S. Kivshar, "Fano resonances in photonics," *Nature Photon.*, vol. 11, no. 9, pp. 543–554, 2017.
- [13] F. Monticone and A. Alù, "Embedded photonic eigenvalues in 3D nanostructures," *Phys. Rev. Lett.*, vol. 112, no. 21, 2014, Art. no. 213903.
- [14] A. Ahmadvand and B. Gerislioglu, "Deep- and vacuum-ultraviolet metaholistic light sources," *Mater. Today*, 2021, doi: [10.1016/j.mattod.2021.05.019](https://doi.org/10.1016/j.mattod.2021.05.019).
- [15] A. Ahmadvand, B. Gerislioglu, R. Ahuja, and Y. K. Mishra, "Toroidal metaholistics and metadevices," *Laser Photon. Rev.*, vol. 14, no. 11, 2020.
- [16] F. Xie, M. Ren, W. Wu, D. Yu, W. Cai, and J. Xu, "Phase-transition optical activity in chiral metasurfaces," *Phys. Rev. Lett.*, vol. 125, no. 23, Dec. 4, 2020, Art. no. 237401.
- [17] F. Xie, W. Wu, M. Ren, W. Cai, and J. Xu, "Lattice collective interaction engineered optical activity in metasurfaces," *Adv. Opt. Mater.*, vol. 8, no. 2, 2019, Art. no. 1901435.
- [18] L. J. Yang, S. Sun, and W. E. I. Sha, "Manipulation of orbital angular momentum spectrum using shape-tailored metasurfaces," *Adv. Opt. Mater.*, vol. 9, no. 2, 2020, Art. no. 2001711.
- [19] H. S. Park, T. T. Kim, H. D. Kim, K. Kim, and B. Min, "Nondispersive optical activity of meshed helical metasurfaces," *Nature Commun.*, vol. 5, Nov. 2014, Art. no. 5435.
- [20] E. Estephan *et al.*, "Sensing by means of nonlinear optics with functionalized GaAs/ALGaAs photonic crystals," *Langmuir*, vol. 26, no. 12, pp. 10373–10379, Jun. 2010.
- [21] G. Pellegrini, M. Finazzi, M. Celebrano, L. Duo, and P. Biagioni, "Surface-enhanced chiroptical spectroscopy with superchiral surface waves," *Chirality*, vol. 30, no. 7, pp. 883–889, Jul. 2018.
- [22] X. Ni, A. V. Kildishev, and V. M. Shalaev, "Metasurface holograms for visible light," *Nature Commun.*, vol. 4, 2013, Art. no. 2807.
- [23] D. Lee, J. Gwak, T. Badloe, S. Palomba, and J. Rho, "Metasurfaces-based imaging and applications: From miniaturized optical components to functional imaging platforms," *Nanoscale Adv.*, vol. 2, no. 2, pp. 605–625, 2020.
- [24] A. M. Mohamed, W. Sabra, A. H. Aly, M. Mobarak, and A. S. Shalaby, "A defective one-dimensional superconducting photonic crystal design for the generation of the fano resonance feature," *Physica Scripta*, vol. 95, no. 11, 2020, Art. no. 115503.
- [25] D. Lin, P. Fan, E. Hasman, and M. L. Brongersma, "Dielectric gradient metasurface optical elements," *Science*, vol. 345, no. 6194, pp. 298–302, Jul. 2014.
- [26] A. Arbabi, Y. Horie, M. Bagheri, and A. Faraon, "Dielectric metasurfaces for complete control of phase and polarization with subwavelength spatial resolution and high transmission," *Nature Nanotechnol.*, vol. 10, no. 11, pp. 937–943, Nov. 2015.
- [27] J. Jin, X. Yin, L. Ni, M. Soljacic, B. Zhen, and C. Peng, "Topologically enabled ultrahigh-Q guided resonances robust to out-of-plane scattering," *Nature*, vol. 574, no. 7779, pp. 501–504, Oct. 2019.
- [28] Y. Yang, C. Peng, Y. Liang, Z. Li, and S. Noda, "Analytical perspective for bound states in the continuum in photonic crystal slabs," *Phys. Rev. Lett.*, vol. 113, no. 3, Jul. 2014, Art. no. 037401.
- [29] A. A. Bogdanov *et al.*, "Bound states in the continuum and fano resonances in the strong mode coupling regime," *Adv. Photon.*, vol. 1, no. 1, 2019, Art. no. 016001.
- [30] O. Kilic, M. Digonnet, G. Kino, and O. Solgaard, "Controlling uncoupled resonances in photonic crystals through breaking the mirror symmetry," *Opt. Exp.*, vol. 16, no. 17, pp. 13090–13103, 2008.
- [31] J. Xia *et al.*, "Turning a hot spot into a cold spot: Polarization-controlled Fano-shaped local-field responses probed by a quantum dot," *Light Sci. Appl.*, vol. 9, 2020, Art. no. 166.